

Measurement of the amplitude ratio of $B^0 \rightarrow D^0 K^{*0}$ and $B^0 \rightarrow \bar{D}^0 K^{*0}$ decays with a model-independent Dalitz plot analysis using $D \rightarrow K_S^0 \pi^+ \pi^-$ decays

A. Abdesselam,⁷⁹ I. Adachi,^{19,15} K. Adamczyk,⁵⁸ H. Aihara,⁸⁵ S. Al Said,^{79,38} K. Arinstein,⁴ Y. Arita,⁵¹ D. M. Asner,⁶⁴ T. Aso,⁹⁰ V. Aulchenko,⁴ T. Aushev,^{50,32} R. Ayad,⁷⁹ T. Aziz,⁸⁰ V. Babu,⁸⁰ I. Badhrees,^{79,37} S. Bahinipati,²³ A. M. Bakich,⁷⁸ A. Bala,⁶⁵ Y. Ban,⁶⁶ V. Bansal,⁶⁴ E. Barberio,⁴⁸ M. Barrett,¹⁸ W. Bartel,⁹ A. Bay,⁴³ I. Bedny,⁴ P. Behera,²⁵ M. Belhorn,⁸ K. Belous,²⁹ V. Bhardwaj,⁵⁴ B. Bhuyan,²⁴ M. Bischofberger,⁵⁴ S. Blyth,⁵⁶ A. Bobrov,⁴ A. Bondar,⁴ G. Bonvicini,⁹³ C. Bookwalter,⁶⁴ A. Bozek,⁵⁸ M. Bračko,^{46,33} J. Brodzicka,⁵⁸ T. E. Browder,¹⁸ D. Červenkov,⁵ M.-C. Chang,¹¹ P. Chang,⁵⁷ Y. Chao,⁵⁷ V. Chekelian,⁴⁷ A. Chen,⁵⁵ K.-F. Chen,⁵⁷ P. Chen,⁵⁷ B. G. Cheon,¹⁷ K. Chilikin,³² R. Chistov,³² K. Cho,³⁹ V. Chobanova,⁴⁷ S.-K. Choi,¹⁶ Y. Choi,⁷⁷ D. Cinabro,⁹³ J. Crnkovic,²² J. Dalseno,^{47,81} M. Danilov,^{32,49} S. Di Carlo,⁹³ J. Dingfelder,³ Z. Doležal,⁵ Z. Drásal,⁵ A. Drutskoy,^{32,49} S. Dubey,¹⁸ D. Dutta,²⁴ K. Dutta,²⁴ S. Eidelman,⁴ D. Epifanov,⁸⁵ S. Esen,⁸ H. Farhat,⁹³ J. E. Fast,⁶⁴ M. Feindt,³⁵ T. Ferber,⁹ A. Frey,¹⁴ O. Frost,⁹ M. Fujikawa,⁵⁴ B. G. Fulsom,⁶⁴ V. Gaur,⁸⁰ N. Gabyshev,⁴ S. Ganguly,⁹³ A. Garmash,⁴ D. Getzkow,¹² R. Gillard,⁹³ F. Giordano,²² R. Glattauer,²⁸ Y. M. Goh,¹⁷ B. Golob,^{44,33} M. Grosse Perdekamp,^{22,71} J. Grygier,³⁵ O. Grzymkowska,⁵⁸ H. Guo,⁷³ J. Haba,^{19,15} P. Hamer,¹⁴ Y. L. Han,²⁷ K. Hara,¹⁹ T. Hara,^{19,15} Y. Hasegawa,⁷⁵ J. Hasenbusch,³ K. Hayasaka,⁵² H. Hayashii,⁵⁴ X. H. He,⁶⁶ M. Heck,³⁵ M. Hedges,¹⁸ D. Heffernan,⁶³ M. Heider,³⁵ A. Heller,³⁵ T. Higuchi,³⁶ S. Himori,⁸⁴ T. Horiguchi,⁸⁴ Y. Horii,⁵² Y. Hoshi,⁸³ K. Hoshina,⁸⁸ W.-S. Hou,⁵⁷ Y. B. Hsiung,⁵⁷ M. Huschle,³⁵ H. J. Hyun,⁴² Y. Igarashi,¹⁹ T. Iijima,^{52,51} M. Imamura,⁵¹ K. Inami,⁵¹ A. Ishikawa,⁸⁴ K. Itagaki,⁸⁴ R. Itoh,^{19,15} M. Iwabuchi,⁹⁵ M. Iwasaki,⁸⁵ Y. Iwasaki,¹⁹ T. Iwashita,³⁶ S. Iwata,⁸⁷ I. Jaegle,¹⁸ M. Jones,¹⁸ K. K. Joo,⁷ T. Julius,⁴⁸ D. H. Kah,⁴² H. Kakuno,⁸⁷ J. H. Kang,⁹⁵ K. H. Kang,⁴² P. Kapusta,⁵⁸ S. U. Kataoka,⁵³ N. Katayama,¹⁹ E. Kato,⁸⁴ Y. Kato,⁵¹ P. Katrenko,³² H. Kawai,⁶ T. Kawasaki,⁶⁰ H. Kichimi,¹⁹ C. Kiesling,⁴⁷ B. H. Kim,⁷⁴ D. Y. Kim,⁷⁶ H. J. Kim,⁴² J. B. Kim,⁴⁰ J. H. Kim,³⁹ K. T. Kim,⁴⁰ M. J. Kim,⁴² S. H. Kim,¹⁷ S. K. Kim,⁷⁴ Y. J. Kim,³⁹ K. Kinoshita,⁸ C. Kleinwort,⁹ J. Klucar,³³ B. R. Ko,⁴⁰ N. Kobayashi,⁸⁶ S. Koblitz,⁴⁷ P. Kodyš,⁵ Y. Koga,⁵¹ S. Korpar,^{46,33} R. T. Kouzes,⁶⁴ P. Križan,^{44,33} P. Krokovny,⁴ B. Kronenbitter,³⁵ T. Kuhr,³⁵ R. Kumar,⁶⁸ T. Kumita,⁸⁷ E. Kurihara,⁶ Y. Kuroki,⁶³ A. Kuzmin,⁴ P. Kvasnička,⁵ Y.-J. Kwon,⁹⁵ Y.-T. Lai,⁵⁷ J. S. Lange,¹² D. H. Lee,⁴⁰ I. S. Lee,¹⁷ S.-H. Lee,⁴⁰ M. Leitgab,^{22,71} R. Leitner,⁵ P. Lewis,¹⁸ J. Li,⁷⁴ X. Li,⁷⁴ Y. Li,⁹² L. Li Gioi,⁴⁷ J. Libby,²⁵ A. Limosani,⁴⁸ C. Liu,⁷³ Y. Liu,⁸ Z. Q. Liu,²⁷ D. Liventsev,⁹² R. Louvot,⁴³ P. Lukin,⁴ J. MacNaughton,¹⁹ D. Matvienko,⁴ A. Matyja,⁵⁸ S. McOnie,⁷⁸ Y. Mikami,⁸⁴ K. Miyabayashi,⁵⁴ Y. Miyachi,⁹⁴ H. Miyake,^{19,15} H. Miyata,⁶⁰ Y. Miyazaki,⁵¹ R. Mizuk,^{32,49} G. B. Mohanty,⁸⁰ S. Mohanty,^{80,91} D. Mohapatra,⁶⁴ A. Moll,^{47,81} H. K. Moon,⁴⁰ T. Mori,⁵¹ H.-G. Moser,⁴⁷ T. Müller,³⁵ N. Muramatsu,⁶⁹ R. Mussa,³¹ T. Nagamine,⁸⁴ Y. Nagasaka,²⁰ Y. Nakahama,⁸⁵ I. Nakamura,^{19,15} K. Nakamura,¹⁹ E. Nakano,⁶² H. Nakano,⁸⁴ T. Nakano,⁷⁰ M. Nakao,¹⁹ H. Nakayama,¹⁹ H. Nakazawa,⁵⁵ T. Nanut,³³ Z. Natkaniec,⁵⁸ M. Nayak,²⁵ E. Nedelkovska,⁴⁷ K. Negishi,⁸⁴ K. Neichi,⁸³ C. Ng,⁸⁵ C. Niebuhr,⁹ M. Niiyama,⁴¹ N. K. Nisar,⁸⁰ S. Nishida,^{19,15} K. Nishimura,¹⁸ O. Nitoh,⁸⁸ T. Nozaki,¹⁹ A. Ogawa,⁷¹ S. Ogawa,⁸² T. Ohshima,⁵¹ S. Okuno,³⁴ S. L. Olsen,⁷⁴ Y. Ono,⁸⁴ Y. Onuki,⁸⁵ W. Ostrowicz,⁵⁸ C. Oswald,³ H. Ozaki,^{19,15} P. Pakhlov,^{32,49} G. Pakhlova,^{50,32} H. Palka,⁵⁸ E. Panzenböck,^{14,54} C.-S. Park,⁹⁵ C. W. Park,⁷⁷ H. Park,⁴² H. K. Park,⁴² K. S. Park,⁷⁷ L. S. Peak,⁷⁸ T. K. Pedlar,⁴⁵ T. Peng,⁷³ L. Pesantez,³ R. Pestotnik,³³ M. Peters,¹⁸ M. Petrić,³³ L. E. Piilonen,⁹² A. Poluektov,⁴ K. Prasanth,²⁵ M. Prim,³⁵ K. Prothmann,^{47,81} C. Pulvermacher,³⁵ B. Reisert,⁴⁷ E. Ribežl,³³ M. Ritter,⁴⁷ M. Röhrken,³⁵ J. Rorie,¹⁸ A. Rostomyan,⁹ M. Rozanska,⁵⁸ S. Ryu,⁷⁴ H. Sahoo,¹⁸ T. Saito,⁸⁴ K. Sakai,¹⁹ Y. Sakai,^{19,15} S. Sandilya,⁸⁰ D. Santel,⁸ L. Santelj,³³ T. Sanuki,⁸⁴ N. Sasao,⁴¹ Y. Sato,⁵¹ V. Savinov,⁶⁷ O. Schneider,⁴³ G. Schnell,^{1,21} P. Schönmeier,⁸⁴ M. Schram,⁶⁴ C. Schwanda,²⁸ A. J. Schwartz,⁸ B. Schwenker,¹⁴ R. Seidl,⁷¹ A. Sekiya,⁵⁴ D. Semmler,¹² K. Senyo,⁹⁴ O. Seon,⁵¹ I. Seong,¹⁸ M. E. Seviar,⁴⁸ L. Shang,²⁷ M. Shapkin,²⁹ V. Shebalin,⁴ C. P. Shen,² T.-A. Shibata,⁸⁶ H. Shibuya,⁸² S. Shinomiya,⁶³ J.-G. Shiu,⁵⁷ B. Shwartz,⁴ A. Sibidanov,⁷⁸ F. Simon,^{47,81} J. B. Singh,⁶⁵ R. Sinha,³⁰ P. Smerkol,³³ Y.-S. Sohn,⁹⁵ A. Sokolov,²⁹ Y. Soloviev,⁹ E. Solovieva,³² S. Stanič,⁶¹ M. Starič,³³ M. Steder,⁹ J. Stypula,⁵⁸ S. Sugihara,⁸⁵ A. Sugiyama,⁷² M. Sumihama,¹³ K. Sumisawa,^{19,15} T. Sumiyoshi,⁸⁷ K. Suzuki,⁵¹ S. Suzuki,⁷² S. Y. Suzuki,¹⁹ Z. Suzuki,⁸⁴ H. Takeichi,⁵¹ U. Tamponi,^{31,89} M. Tanaka,^{19,15} S. Tanaka,^{19,15} K. Tanida,⁷⁴ N. Taniguchi,¹⁹ G. Tatishvili,⁶⁴ G. N. Taylor,⁴⁸ Y. Teramoto,⁶² F. Thorne,²⁸ I. Tikhomirov,³²

K. Trabelsi,^{19,15} V. Trusov,³⁵ Y. F. Tse,⁴⁸ T. Tsuboyama,^{19,15} M. Uchida,⁸⁶ T. Uchida,¹⁹ Y. Uchida,¹⁵ S. Uehara,^{19,15} K. Ueno,⁵⁷ T. Uglov,^{32,50} Y. Unno,¹⁷ S. Uno,^{19,15} P. Urquijo,⁴⁸ Y. Ushiroda,^{19,15} Y. Usov,⁴ S. E. Vahsen,¹⁸ C. Van Hulse,¹ P. Vanhoefer,⁴⁷ G. Varner,¹⁸ K. E. Varvell,⁷⁸ K. Vervink,⁴³ A. Vinokurova,⁴ V. Vorobyev,⁴ A. Vossen,²⁶ M. N. Wagner,¹² C. H. Wang,⁵⁶ J. Wang,⁶⁶ M.-Z. Wang,⁵⁷ P. Wang,²⁷ X. L. Wang,⁹² M. Watanabe,⁶⁰ Y. Watanabe,³⁴ R. Wedd,⁴⁸ S. Wehle,⁹ E. White,⁸ J. Wiechczynski,⁵⁸ K. M. Williams,⁹² E. Won,⁴⁰ B. D. Yabsley,⁷⁸ S. Yamada,¹⁹ H. Yamamoto,⁸⁴ J. Yamaoka,⁶⁴ Y. Yamashita,⁵⁹ M. Yamauchi,^{19,15} S. Yashchenko,⁹ J. Yelton,¹⁰ Y. Yook,⁹⁵ C. Z. Yuan,²⁷ Y. Yusa,⁶⁰ C. C. Zhang,²⁷ L. M. Zhang,⁷³ Z. P. Zhang,⁷³ L. Zhao,⁷³ V. Zhilich,⁴ V. Zhulanov,⁴ M. Ziegler,³⁵ T. Zivko,³³ A. Zupanc,³³ N. Zwahlen,⁴³ and O. Zyukova⁴

(The Belle Collaboration)

¹University of the Basque Country UPV/EHU, 48080 Bilbao

²Beihang University, Beijing 100191

³University of Bonn, 53115 Bonn

⁴Budker Institute of Nuclear Physics SB RAS and Novosibirsk State University, Novosibirsk 630090

⁵Faculty of Mathematics and Physics, Charles University, 121 16 Prague

⁶Chiba University, Chiba 263-8522

⁷Chonnam National University, Kwangju 660-701

⁸University of Cincinnati, Cincinnati, Ohio 45221

⁹Deutsches Elektronen-Synchrotron, 22607 Hamburg

¹⁰University of Florida, Gainesville, Florida 32611

¹¹Department of Physics, Fu Jen Catholic University, Taipei 24205

¹²Justus-Liebig-Universität Gießen, 35392 Gießen

¹³Gifu University, Gifu 501-1193

¹⁴II. Physikalisches Institut, Georg-August-Universität Göttingen, 37073 Göttingen

¹⁵The Graduate University for Advanced Studies, Hayama 240-0193

¹⁶Gyeongsang National University, Chinju 660-701

¹⁷Hanyang University, Seoul 133-791

¹⁸University of Hawaii, Honolulu, Hawaii 96822

¹⁹High Energy Accelerator Research Organization (KEK), Tsukuba 305-0801

²⁰Hiroshima Institute of Technology, Hiroshima 731-5193

²¹IKERBASQUE, Basque Foundation for Science, 48013 Bilbao

²²University of Illinois at Urbana-Champaign, Urbana, Illinois 61801

²³Indian Institute of Technology Bhubaneswar, Satya Nagar 751007

²⁴Indian Institute of Technology Guwahati, Assam 781039

²⁵Indian Institute of Technology Madras, Chennai 600036

²⁶Indiana University, Bloomington, Indiana 47408

²⁷Institute of High Energy Physics, Chinese Academy of Sciences, Beijing 100049

²⁸Institute of High Energy Physics, Vienna 1050

²⁹Institute for High Energy Physics, Protvino 142281

³⁰Institute of Mathematical Sciences, Chennai 600113

³¹INFN - Sezione di Torino, 10125 Torino

³²Institute for Theoretical and Experimental Physics, Moscow 117218

³³J. Stefan Institute, 1000 Ljubljana

³⁴Kanagawa University, Yokohama 221-8686

³⁵Institut für Experimentelle Kernphysik, Karlsruher Institut für Technologie, 76131 Karlsruhe

³⁶Kavli Institute for the Physics and Mathematics of the Universe (WPI), University of Tokyo, Kashiwa 277-8583

³⁷King Abdulaziz City for Science and Technology, Riyadh 11442

³⁸Department of Physics, Faculty of Science, King Abdulaziz University, Jeddah 21589

³⁹Korea Institute of Science and Technology Information, Daejeon 305-806

⁴⁰Korea University, Seoul 136-713

⁴¹Kyoto University, Kyoto 606-8502

⁴²Kyungpook National University, Daegu 702-701

⁴³École Polytechnique Fédérale de Lausanne (EPFL), Lausanne 1015

⁴⁴Faculty of Mathematics and Physics, University of Ljubljana, 1000 Ljubljana

⁴⁵Luther College, Decorah, Iowa 52101

⁴⁶University of Maribor, 2000 Maribor

⁴⁷Max-Planck-Institut für Physik, 80805 München

⁴⁸School of Physics, University of Melbourne, Victoria 3010

⁴⁹Moscow Physical Engineering Institute, Moscow 115409

⁵⁰Moscow Institute of Physics and Technology, Moscow Region 141700

⁵¹Graduate School of Science, Nagoya University, Nagoya 464-8602

⁵²Kobayashi-Maskawa Institute, Nagoya University, Nagoya 464-8602

- ⁵³Nara University of Education, Nara 630-8528
⁵⁴Nara Women's University, Nara 630-8506
⁵⁵National Central University, Chung-li 32054
⁵⁶National United University, Miao Li 36003
⁵⁷Department of Physics, National Taiwan University, Taipei 10617
⁵⁸H. Niewodniczanski Institute of Nuclear Physics, Krakow 31-342
⁵⁹Nippon Dental University, Niigata 951-8580
⁶⁰Niigata University, Niigata 950-2181
⁶¹University of Nova Gorica, 5000 Nova Gorica
⁶²Osaka City University, Osaka 558-8585
⁶³Osaka University, Osaka 565-0871
⁶⁴Pacific Northwest National Laboratory, Richland, Washington 99352
⁶⁵Panjab University, Chandigarh 160014
⁶⁶Peking University, Beijing 100871
⁶⁷University of Pittsburgh, Pittsburgh, Pennsylvania 15260
⁶⁸Punjab Agricultural University, Ludhiana 141004
⁶⁹Research Center for Electron Photon Science, Tohoku University, Sendai 980-8578
⁷⁰Research Center for Nuclear Physics, Osaka University, Osaka 567-0047
⁷¹RIKEN BNL Research Center, Upton, New York 11973
⁷²Saga University, Saga 840-8502
⁷³University of Science and Technology of China, Hefei 230026
⁷⁴Seoul National University, Seoul 151-742
⁷⁵Shinshu University, Nagano 390-8621
⁷⁶Soongsil University, Seoul 156-743
⁷⁷Sungkyunkwan University, Suwon 440-746
⁷⁸School of Physics, University of Sydney, NSW 2006
⁷⁹Department of Physics, Faculty of Science, University of Tabuk, Tabuk 71451
⁸⁰Tata Institute of Fundamental Research, Mumbai 400005
⁸¹Excellence Cluster Universe, Technische Universität München, 85748 Garching
⁸²Toho University, Funabashi 274-8510
⁸³Tohoku Gakuin University, Tagajo 985-8537
⁸⁴Tohoku University, Sendai 980-8578
⁸⁵Department of Physics, University of Tokyo, Tokyo 113-0033
⁸⁶Tokyo Institute of Technology, Tokyo 152-8550
⁸⁷Tokyo Metropolitan University, Tokyo 192-0397
⁸⁸Tokyo University of Agriculture and Technology, Tokyo 184-8588
⁸⁹University of Torino, 10124 Torino
⁹⁰Toyama National College of Maritime Technology, Toyama 933-0293
⁹¹Utkal University, Bhubaneswar 751004
⁹²CNP, Virginia Polytechnic Institute and State University, Blacksburg, Virginia 24061
⁹³Wayne State University, Detroit, Michigan 48202
⁹⁴Yamagata University, Yamagata 990-8560
⁹⁵Yonsei University, Seoul 120-749

We report a measurement of the amplitude ratio r_S of $B^0 \rightarrow D^0 K^{*0}$ and $B^0 \rightarrow \bar{D}^0 K^{*0}$ decays with a model-independent Dalitz plot analysis using $D \rightarrow K_S^0 \pi^+ \pi^-$ decays. Using the full data sample of 772×10^6 $B\bar{B}$ pairs collected at the $\Upsilon(4S)$ resonance with the Belle detector at KEKB accelerator the upper limit is $r_S < 0.87$ at the 68 % confidence level. This result is the first measurement of r_S with a model-independent Dalitz analysis, and is consistent with results from other analyses. The value of r_S indicates the sensitivity of the decay to ϕ_3 because the statistical uncertainty is proportional to $1/r_S$. The r_S result is obtained from observables (x_{\pm}, y_{\pm})

$$\begin{aligned} x_- &= +0.4_{-0.6-0.1}^{+1.0+0.0} \pm 0.0 \\ y_- &= -0.6_{-1.0-0.0}^{+0.8+0.1} \pm 0.1 \\ x_+ &= +0.1_{-0.4-0.1}^{+0.7+0.0} \pm 0.1 \\ y_+ &= +0.3_{-0.8-0.1}^{+0.5+0.0} \pm 0.1, \end{aligned}$$

where $x_{\pm} = r_S \cos(\delta_S \pm \phi_3)$, $y_{\pm} = r_S \sin(\delta_S \pm \phi_3)$ and ϕ_3 (δ_S) are the weak (strong) phase difference between $B^0 \rightarrow D^0 K^{*0}$ and $B^0 \rightarrow \bar{D}^0 K^{*0}$. The first uncertainty is statistical, the second is the experimental systematic and the third is the systematic due to the uncertainties on c_i and s_i parameters measured by CLEO.

INTRODUCTION

Determination of the parameters of the standard model (SM) plays an important role in the search for new physics. In the SM, the Cabibbo-Kobayashi-Maskawa (CKM) matrix [1] gives a successful description of current measurements of CP violation. CP -violating parameters ϕ_1 , ϕ_2 and ϕ_3 are the three angles of a CKM unitarity triangle, of which $\phi_3 \equiv \arg(-V_{ud}V_{ub}^*/V_{cd}V_{cb}^*)$ is the least accurately determined. In the usual quark-phase convention, where large complex phases appear only in V_{ub} and V_{td} [2], the measurement of ϕ_3 is equivalent to the extraction of the phase of V_{ub} relative to the phases of the other CKM matrix elements except V_{td} . To date, ϕ_3 measurements have been made mainly with B meson decays into $D^{(*)}K^{(*)}$ final states [3–12], which exploit the interference between the $\bar{D}^{(*)0}$ and $D^{(*)0}$ decaying into a common final state. In particular, Dalitz plot analyses of D decays in $B^\pm \rightarrow D^{(*)}K^{(*)\pm}$ processes are the most sensitive to ϕ_3 at e^+e^- B-factories. The Dalitz plot analysis technique for the measurement of ϕ_3 was proposed in Ref. [13]. Belle reported the first ϕ_3 measurement with model-independent Dalitz analysis technique [14].

In this paper, we present the first measurement of the amplitude ratio of $B^0 \rightarrow D^0 K^{*0}$ and $B^0 \rightarrow \bar{D}^0 K^{*0}$ decays with a model-independent Dalitz plot analysis, which is essential for the determination of ϕ_3 from this channel. We reconstruct $B^0 \rightarrow DK^{*0}$, with $K^{*0} \rightarrow K^+\pi^-$ (charge conjugate processes are implied throughout the paper and K^{*0} refers to $K^*(892)^0$). Here the flavor of the B meson is identified by the kaon charge. Neutral D mesons are reconstructed in the $K_S^0\pi^+\pi^-$ decay mode. The final states we reconstructed can be reached through $b \rightarrow c$ and $b \rightarrow u$ processes with the diagrams shown in Fig. 1.

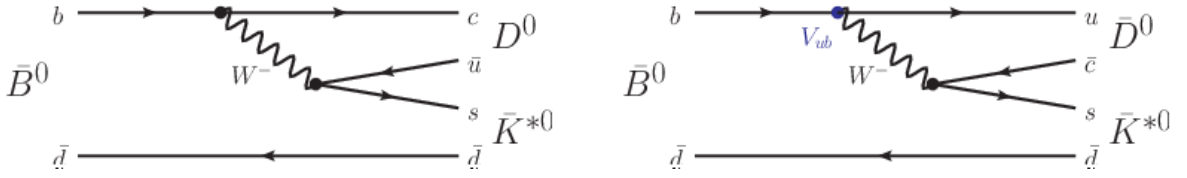


FIG. 1: Diagrams for the $\bar{B}^0 \rightarrow \bar{D}^0 \bar{K}^{*0}$ and $\bar{B}^0 \rightarrow D^0 \bar{K}^{*0}$ decays.

Since the K^* has a large natural width of 50 MeV, we consider interference between the signal $B \rightarrow DK^*$ and $B \rightarrow DK\pi$ where $K\pi$ arises from a non-resonant decay or through other kaonic resonances. In this analysis we use the variables r_S , k , and δ_S to parametrize the strong dynamics of the decay. These parameters are defined as [15]

$$r_S^2 \equiv \frac{\Gamma(B^0 \rightarrow D^0 K^+ \pi^-)}{\Gamma(B^0 \rightarrow \bar{D}^0 K^+ \pi^-)} = \frac{\int dp A_{b \rightarrow u}^2(p)}{\int dp A_{b \rightarrow c}^2(p)}, \quad (1)$$

$$k e^{i\delta_S} \equiv \frac{\int dp A_{b \rightarrow c}(p) A_{b \rightarrow u}(p) e^{i\delta(p)}}{\sqrt{\int dp A_{b \rightarrow c}^2(p) \int dp A_{b \rightarrow u}^2(p)}}, \quad (2)$$

where the integration is over the $B^0 \rightarrow DK^+\pi^-$ Dalitz plot region corresponding to the K^{*0} resonance. Here $A_{b \rightarrow c}(A_{b \rightarrow u})(p)$ are the magnitudes of the amplitudes for the $b \rightarrow c(u)$ transitions, and $\delta(p)$ is the relative strong phase, where the variable p indicates the position within the $DK^+\pi^-$ Dalitz plot. If the B^0 decay can be considered as a DK^{*0} two-body decay, r_S becomes the ratio of the amplitudes for $b \rightarrow u$ and $b \rightarrow c$ and k becomes 1. According to a simulation study using a Dalitz model based on the measurements [16], the value of k is 0.95 ± 0.03 within the phase space of DK^{*0} resonance. The value of r_S is expected to be around 0.4, which naively corresponds to $|V_{ub}V_{cs}^*|/|V_{cb}V_{us}^*|$, but also depends on strong interaction effects.

THE MODEL-INDEPENDENT DALITZ PLOT ANALYSIS TECHNIQUE

The amplitude of the $B^0 \rightarrow DK^{*0}$, $D \rightarrow K_S^0\pi^+\pi^-$ decay is a superposition of the $B^0 \rightarrow \bar{D}^0 K^{*0}$ and $B^0 \rightarrow D^0 K^{*0}$ amplitudes

$$A_B(m_+^2, m_-^2) = \bar{A} + r_S e^{i(\delta_S + \phi_3)} A, \quad (3)$$

where m_+^2 and m_-^2 are the squared invariant masses of $K_S^0\pi^+$ and $K_S^0\pi^-$ combinations, respectively, $\bar{A} = \bar{A}(m_+^2, m_-^2)$ is the amplitude of the $\bar{D}^0 \rightarrow K_S^0\pi^+\pi^-$ decay and $A = A(m_+^2, m_-^2)$ is the amplitude of the $D^0 \rightarrow K_S^0\pi^+\pi^-$ decay. In the case of CP conservation in the D decay $A(m_+^2, m_-^2) = \bar{A}(m_-^2, m_+^2)$. The Dalitz plot density of the D decay from $B^0 \rightarrow DK^{*0}$ is given by

$$P_B = |A_B|^2 = |\bar{A} + r_S e^{i(\delta_S + \phi_3)} A|^2 = \bar{P} + r_S^2 P + 2k\sqrt{P\bar{P}}(x_+ C + y_+ S), \quad (4)$$

where $P(m_+^2, m_-^2) = |A|^2$, $\bar{P}(m_+^2, m_-^2) = |\bar{A}|^2$, and

$$x_+ = r_S \cos(\delta_S + \phi_3), \quad y_+ = r_S \sin(\delta_S + \phi_3). \quad (5)$$

Functions $C = C(m_+^2, m_-^2)$ and $S = S(m_+^2, m_-^2)$ are the cosine and sine of the strong-phase difference $\delta_D(m_+^2, m_-^2) = \arg \bar{A} - \arg A$ between the $\bar{D}^0 \rightarrow K_S^0\pi^+\pi^-$ and $D^0 \rightarrow K_S^0\pi^+\pi^-$ amplitudes. Here, we have used the definition of k given in Eq. (2). The equations for the charge-conjugate mode $\bar{B}^0 \rightarrow D\bar{K}^{*0}$ are obtained with the substitution $\phi_3 \leftrightarrow -\phi_3$ and $A \leftrightarrow \bar{A}$; the corresponding parameters that depend on the \bar{B}^0 decay amplitude are:

$$x_- = r_S \cos(\delta_S - \phi_3), \quad y_- = r_S \sin(\delta_S - \phi_3). \quad (6)$$

Using B^0 and \bar{B}^0 decays, one can obtain r_S , ϕ_3 and δ_S separately.

Up to this point, the description of the model-dependent and model-independent techniques is the same. The model-dependent analysis deals directly with the Dalitz plot density, and the functions C and S are obtained from a model based upon a fit to the $D^0 \rightarrow K_S^0\pi^+\pi^-$ amplitude. In the model-independent approach, the Dalitz plot is divided into $2\mathcal{N}$ bins symmetric under the exchange $m_-^2 \leftrightarrow m_+^2$. The bin index i ranges from $-\mathcal{N}$ to \mathcal{N} (excluding 0); the exchange $m_-^2 \leftrightarrow m_+^2$ corresponds to the exchange $i \leftrightarrow -i$. The expected number of events in bin i of the Dalitz plot of the D meson from $B^0 \rightarrow DK^{*0}$ is

$$N_i^\pm = h_B \left[K_{\pm i} + r_S^2 K_{\mp i} + 2k\sqrt{K_i K_{-i}}(x_\pm c_i \pm y_\pm s_i) \right], \quad (7)$$

where $N^{+(-)}$ stands for the number of $B^0(\bar{B}^0)$ meson decays, h_B is a normalization constant and K_i is the number of events in the i^{th} bin of the $K_S^0\pi^+\pi^-$ Dalitz plot of the D meson. The values of K_i are measured from a sample of flavor-tagged D^0 mesons obtained by reconstructing $D^{*\pm} \rightarrow D\pi^\pm$ decays. The terms c_i and s_i are the amplitude-weighted average of the functions C and S over the bin region:

$$c_i = \frac{\int_{\mathcal{D}_i} |A| |\bar{A}| C d\mathcal{D}}{\sqrt{\int_{\mathcal{D}_i} |A|^2 d\mathcal{D} \int_{\mathcal{D}_i} |\bar{A}|^2 d\mathcal{D}}}. \quad (8)$$

Here \mathcal{D} represents the Dalitz plot plane and \mathcal{D}_i is the bin region over which the integration is performed. The terms s_i are defined similarly with C substituted by S . The absence of CP violation in the D decay implies $c_i = c_{-i}$ and $s_i = -s_{-i}$. The values of c_i and s_i can be measured using quantum correlated D pairs produced at charm-factory experiments operating at the threshold for $D\bar{D}$ pair production. The CLEO Collaboration has reported c_i and s_i values [17, 18]. Once the c_i and s_i measurements are included, the set of relations defined by Eq. (7) contain only three free parameters (x , y , and h_B) for each B^0 , and can be solved using a maximum likelihood method to extract the values of ϕ_3 , δ_S and r_S . We have neglected charm-mixing effects in D decays from both the $B^0 \rightarrow DK^{*0}$ process and in the quantum correlated $D\bar{D}$ production.

In principle, the set of relations defined by Eq. (7) can be solved without external constraints on c_i and s_i for $\mathcal{N} \geq 2$. However, due to the small value of r_S , there is very little sensitivity to the c_i and s_i parameters in $B^0 \rightarrow DK^{*0}$ decays, which results in a reduction in the precision on the other parameters [19].

ANALYSIS PROCEDURE

Equation (7) is the key relation used in the analysis, but it only holds if there is no background, no non-uniformity in the Dalitz plot acceptance and no crossfeed between bins. (Cross-feed is due to invariant-mass resolution and radiative corrections.) In this section we outline the procedures to account for the acceptance and crossfeed.

First we discuss the effect of the variation of efficiency profile over the Dalitz plane. We note that Eq. (4) does not change under the transformation $P \rightarrow \epsilon P$ when the efficiency profile $\epsilon(m_+^2, m_-^2)$ is symmetric: $\epsilon(m_+^2, m_-^2) = \epsilon(m_-^2, m_+^2)$. The effect of non-uniform efficiency over the Dalitz plot cancels out when using a flavor-tagged D sample

with kinematic properties that are similar to the sample from the signal B decay. This approach allows for the removal of the systematic uncertainty associated with the possible inaccuracy of the detector acceptance description in the Monte Carlo (MC) simulation. With the efficiency taken into account (that is in general non-uniform across the bin region), the number of events detected is:

$$N' = \int p(\mathcal{D})\epsilon(\mathcal{D})d\mathcal{D}. \quad (9)$$

Clearly, the efficiency does not factorize. One can use an efficiency averaged over the bin then correct for it in the analysis:

$$\bar{\epsilon}_i = \frac{N'_i}{N_i} = \frac{\int p(\mathcal{D})\epsilon(\mathcal{D})d\mathcal{D}}{\int p(\mathcal{D})d\mathcal{D}} \quad (10)$$

The averaged efficiency $\bar{\epsilon}_i$ can be determined from MC. The assumption that the efficiency profile depends only on the D momentum is tested using MC simulation, and the remaining difference is treated as a systematic uncertainty. This correction cannot be performed in a completely model-independent way, since the correction terms include the amplitude variation inside the bin. Fortunately, calculations using the Belle $D \rightarrow K_S^0 \pi^+ \pi^-$ model [20] show that this correction is negligible even for very large non-uniformity of the efficiency profile.

There are two sources of cross-feed: momentum resolution and flavor misidentification. Momentum resolution leads to migration of events between the bins. In the binned approach, this effect can be corrected in a non-parametric way. The migration can be described by a linear transformation of the number of events in each bin

$$N'_i = \sum \alpha_{ik} N_k, \quad (11)$$

where N_k is the number of events that bin k would contain without the cross-feed, and N'_i is the reconstructed number of events in bin i . The crossfeed matrix α_{ik} is nearly a unit matrix: $\alpha_{ik} \ll 1$ for $i \neq k$. The matrix is obtained from a signal MC simulation generated with the amplitude model reported in Ref. [20]. Most of the off-diagonal elements are null, only a few have values $\alpha_{ik} \leq 0.04$. In the case of a $D \rightarrow K_S^0 \pi^+ \pi^-$ decay from a B , the cross-feed depends on the parameters x and y . However, this is a minor correction to an already small effect due to cross-feed; therefore it is neglected.

The final effect to be considered are events in which the B flavor is misidentified. Double mis-identification in K^{*0} reconstruction from $K^+ \pi^-$, leads to migration of events between $N_i^+ \leftrightarrow N_{-i}^-$, due to assignment of the wrong flavor to the B candidate. If the fraction of double mis-identified events is β , the number of events in each bin can be written as

$$N_i'^{\pm} = N_i^{\pm} + \beta N_{-i}^{\mp}. \quad (12)$$

The value of β is obtained from MC data and is found to be $(0.119 \pm 0.007)\%$. Therefore, in this analysis the effect of flavor misidentification is neglected.

Fit Procedure

We can fit the data distribution in each bin separately, with the number of signal and background events as free parameters. The values of N_i found can be used in Eq. (7) to obtain the parameters (x_{\pm}, y_{\pm}) . This is accomplished by minimizing a negative logarithmic likelihood of the form

$$-2 \log \mathcal{L}(x, y) = -2 \sum_i \log p(\langle N_i \rangle(x, y), N_i, \sigma_{N_i}), \quad (13)$$

where $\langle N_i \rangle$ is the expected number of events in the bin i obtained from Eq. (7). Here, N_i and σ_{N_i} are the observed number of events in data and the uncertainty on N_i , respectively. If the probability density function (PDF) p is Gaussian, this procedure is equivalent to a χ^2 fit; however, the assumption of the Gaussian distribution may introduce a bias in the case of low statistics in certain bins.

The procedure described above does not make any assumptions on the Dalitz distribution of the background events, since the fits in each bin are independent. Thus there is no associated systematic uncertainty. However, in the case of a small number of events and many background components this can be a limiting factor. Our approach is to

use the combined fit with a common likelihood for all bins. The background contribution has to be accounted for in the calculation of the values N_i . Statistically the most effective way of calculating the number of signal events is to perform, in each bin i of the Dalitz plot, an unbinned fit in the variables used to distinguish the signal from the background. In this analysis, we obtain the CP violating parameters (x_{\pm}, y_{\pm}) from the data from a combined fit in bins. The relative numbers of background events in the bins of such a fit can be constrained externally from MC samples. In the combined fit, the expected numbers of events $\langle N_i \rangle$ as functions of (x, y) can be included in the likelihood. Thus the variables (x, y) become free parameters of the combined likelihood fit, and the assumption that the number of signal events has a Gaussian distribution is not needed.

EVENT RECONSTRUCTION AND SELECTION

This analysis is based on a data sample that contains 772×10^6 $B\bar{B}$ pairs, collected with the Belle detector at the KEKB asymmetric-energy e^+e^- (3.5 on 8 GeV) collider [21] operating at the $\Upsilon(4S)$ resonance. The Belle detector is a large-solid-angle magnetic spectrometer that consists of a silicon vertex detector, a 50-layer central drift chamber (CDC), an array of aerogel threshold Cherenkov counters (ACC), a barrel-like arrangement of time-of-flight scintillation counters (TOF), and an electromagnetic calorimeter comprised of CsI(Tl) crystals located inside a superconducting solenoid coil that provides a 1.5 T magnetic field. An iron flux-return located outside of the coil is instrumented to detect K_L^0 mesons and to identify muons. The detector is described in detail elsewhere [22].

We reconstructed $B^0 \rightarrow DK^{*0}$ events with $K^{*0} \rightarrow K^+\pi^-$ and $D \rightarrow K_S^0\pi^+\pi^-$. The event selection, described below, is developed from studies of off-resonance data and MC simulated events.

The K_S^0 candidates are identified using the output of a neural network. Inputs to the network for a pair of oppositely-charged pions are the invariant mass, 20 kinematic parameters and particle identification (PID) information from the ACC, TOF and the ionization energy loss in the CDC. The K_S^0 selection has a simulated purity of 92.2% and an efficiency of 75.1%. Charged kaon and pion candidates are identified using PID information. The efficiency is 85–95% and the probability of misidentification is 10–20% depending upon the momentum of the hadrons as obtained using dedicated data control samples. We reconstruct neutral D mesons by combining a K_S^0 candidate with a pair of oppositely-charged pion candidates. We require that the invariant mass is within ± 15 MeV/ c^2 ($\pm 3\sigma$) of the nominal D^0 mass. K^{*0} candidates are reconstructed from $K^+\pi^-$ pairs. We require that the invariant mass is within ± 50 MeV/ c^2 of the nominal K^{*0} mass. We combine D and K^{*0} candidates to form B^0 mesons. Candidate events are identified by the energy difference $\Delta E \equiv \sum_i E_i - E_b$ and the beam-constrained mass $M_{bc} \equiv \sqrt{E_b^2 - |\sum_i \vec{p}_i|^2}$, where E_b is the beam energy and \vec{p}_i and E_i are the momenta and energies, respectively, of the B^0 meson decay products in the e^+e^- center-of-mass (CM) frame. We select events with $5.2 \text{ GeV}/c^2 < M_{bc} < 5.29 \text{ GeV}/c^2$ and $-0.1 \text{ GeV} < \Delta E < 0.15 \text{ GeV}$.

Among other B decays, the most serious background is from $\bar{B}^0 \rightarrow [\bar{K}^{*0}\pi^+]_{D^+}[K^0\pi^-]_{K^{*-}}$. This decay produces the same final state as the $B^0 \rightarrow DK^{*0}$ signal. To suppress this background, we exclude candidates for which the invariant mass of the $K^{*0}\pi^+$ system is within ± 4 MeV/ c^2 of the nominal D^+ mass. This criteria leads to negligible contamination from $\bar{B}^0 \rightarrow [\bar{K}^{*0}\pi^+]_{D^+}[K^0\pi^-]_{K^{*-}}$ and a relative loss in the signal efficiency of 0.6%.

Large combinatorial background of true D^0 and random K^+ and π^- combinations from the $e^+e^- \rightarrow c\bar{c}$ process and other $B\bar{B}$ decays is reduced if D^0 candidates that are a decay product of $D^{*+} \rightarrow D^0\pi^+$ are eliminated. We use the mass difference ΔM between the $[K_S^0\pi^+\pi^-]_{D^0\pi^+}$ and $[K_S^0\pi^+\pi^-]_D$ systems. If $\Delta M > 0.15 \text{ GeV}/c^2$ for any additional π^+ candidate not used in the B candidate reconstruction, the event is retained. This requirement removes 19% of $c\bar{c}$ background and 11% of $B\bar{B}$ background according to MC simulation. The relative loss in signal efficiency is 5.5%.

In the rare case where there are multiple candidates in an event, the candidate with M_{bc} closest to its nominal value is chosen. The relative loss in signal efficiency is 0.8%.

To discriminate the large combinatorial background dominated by the two-jet-like $e^+e^- \rightarrow q\bar{q}$ continuum process, where q indicates u, d, s or c , a multivariate analysis is performed using the 12 variables introduced in the Table I. To effectively combine these 12 variables, we employ the NeuroBayes neural network package [25]. The NeuroBayes output is denoted as C_{NB} and lies within the range $[-1, 1]$. Events with $C_{NB} \sim 1$ are signal-like and events with $C_{NB} \sim -1$ are $q\bar{q}$ -like. The training of the neural network is performed using signal and $q\bar{q}$ MC samples. The C_{NB} distribution of signal events peaks at $|C_{NB}| \sim 1$ and is therefore difficult to represent with a simple analytic function. However, the transformed variable

$$C'_{NB} = \ln \frac{C_{NB} - C_{NB,low}}{C_{NB,high} - C_{NB}}, \quad (14)$$

1	Fisher discriminants based on modified Fox-Wolfram moments [23].
2	The angle in the CM frame between the thrust axes of the B decay and that of remaining particles.
3	The signed difference of the vertices between the B candidate and the remaining charged tracks.
4	The distance of closest approach between the trajectories of the K^* and D candidates.
5	The expected flavor dilution factor described in Ref. [24].
6	The angle θ between the B meson momentum direction and the beam axis in the CM frame.
7	The angle between the D and $\Upsilon(4S)$ directions in the rest frame of the B candidate.
8	The projection on to the e^+e^- beam direction of the sphericity vector with the largest eigenvalue.
9	The angle of the sphericity vector of the signal with respect to that of the remaining particles with the largest eigenvalue.
10	The angle of the sphericity vector of the signal with respect to the remaining particles with the second largest eigenvalue.
11	The angle of sphericity vector from the signal with respect to the remaining particles with the smallest eigenvalue.
12	The magnitude of the thrust of the particles not used to reconstruct the signal.

TABLE I: 12 variables for $q\bar{q}$ suppression.

where $C_{\text{NB,low}} = -0.6$ and $C_{\text{NB,high}} = 0.9992$, has a distribution that can be modelled by a Gaussian for signal as well as background. The events with $C_{\text{NB}} < -0.6$ are rejected.

The number of signal events is obtained by fitting the three-dimensional distribution of variables M_{bc} , ΔE , and C'_{NB} using the extended maximum likelihood method. We prepare three-dimensional PDFs for each component by forming the product of one-dimensional PDFs for ΔE , M_{bc} and C'_{NB} , since the correlations among the variables are found to be small.

Backgrounds are divided into the following components:

- Combinatorial background from $q\bar{q}$ background events.
- $B\bar{B}$ background, in which the tracks forming the $B^0 \rightarrow DK^{*0}$ candidate come from decays of both B mesons in the event. The number of possible B decay combinations that contribute to this background is large, therefore both the Dalitz distribution and fit parameters distribution are quite smooth. In this analysis, $B\bar{B}$ backgrounds are further subdivided into two components: events reconstructed with a true $D \rightarrow K_S^0 \pi^+ \pi^-$ decay, referred to as D true, and those reconstructed with a combinatorial D candidate, referred to as D fake.
- Peaking $B\bar{B}$ background, in which all tracks forming the $B^0 \rightarrow DK^{*0}$ candidate come from the same B meson. This background has two types: events with one pion misidentified as a kaon, such as $D^0[\pi^+ \pi^-]_{\rho^0}$; and one pion misidentified as a kaon and one pion is not reconstructed, such as $D^0[\pi^+ \pi^+ \pi^-]_{a_1^+}$.

The ΔE PDFs are parameterized by a double Gaussian for the signal, an exponential function for the D true $B\bar{B}$ background, an exponential function for the D fake $B\bar{B}$ background, a linear function for the $q\bar{q}$ background, a double Gaussian for the $\bar{D}^0 \rho^0$ background, and a Gaussian for the $\bar{D}^0 a_1^+$ background. The M_{bc} PDFs are a Gaussian for signal, a Crystal Ball function for D true $B\bar{B}$ background, an Argus function for D fake $B\bar{B}$ background, an Argus function for $q\bar{q}$ background, a sum of Gaussian and Argus function for $\bar{D}^0 \rho^0$ background and a Gaussian for $\bar{D}^0 a_1^+$ background. The C'_{NB} PDF are a sum of Gaussian and bifurcated Gaussian for each component. The shape parameters of the PDFs are fixed from MC samples.

The Dalitz plot distributions of the background components are discussed in the next section. The numbers of events in each bin can be free parameters in the fit, thus there will be no uncertainty due to the modeling of the background distribution over the Dalitz plot in such an approach. This procedure is justified for background that is either well separated from the signal (such as peaking $B\bar{B}$ background), or is constrained by a much larger number of events than the signal (such as the $q\bar{q}$ background). The results of the fit over the full Dalitz plot are shown in Figs. 2. We obtain a total of $44.2^{+13.3}_{-12.1}$ signal events. The statistical significance is 2.8σ .

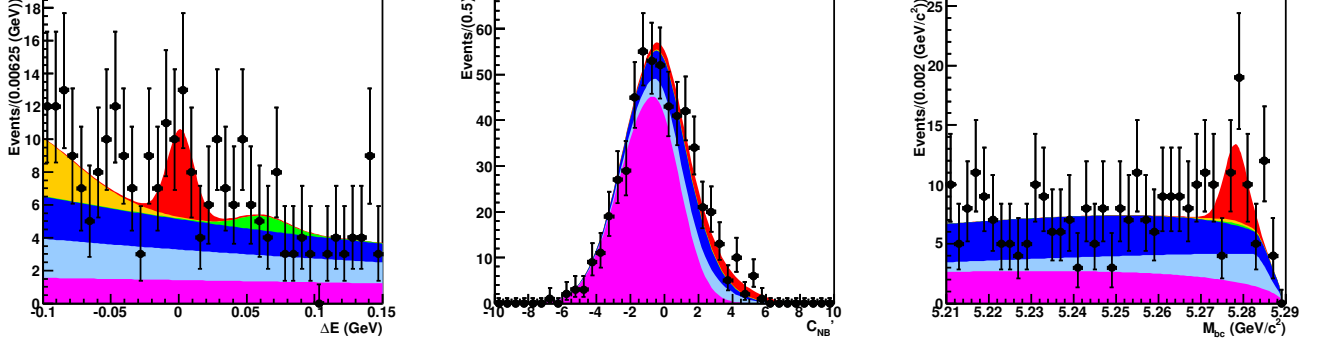


FIG. 2: Projection of the fit to real data using the full Dalitz plot. Left: ΔE distribution with $M_{bc} > 5.270 \text{ GeV}/c^2$ and $C'_{NB} > 2$ requirements. Middle: C'_{NB} distribution with $|\Delta E| < 0.030 \text{ GeV}$ and $M_{bc} > 5.270 \text{ GeV}/c^2$ requirements. Right: M_{bc} distribution with $|\Delta E| < 0.030 \text{ GeV}$ and $C'_{NB} > 2$ requirements. Histograms show the fitted signal and background contributions, (red is signal, yellow is $D^0 a_1^+$, green is $D^0 \rho^0$, blue is D fake $B\bar{B}$, light blue is D true $B\bar{B}$ and magenta is $q\bar{q}$) and points with error bars are the data.

Parameter	
x_-	$+0.29 \pm 0.32$
y_-	-0.33 ± 0.41
corr. (x_-, y_-)	$+7.0\%$
x_+	$+0.07 \pm 0.42$
y_+	$+0.05 \pm 0.45$
corr. (x_+, y_+)	-7.5%

TABLE II: (x, y) parameters and their statistical correlations from combined fit of the $B^0 \rightarrow DK^{*0}$ sample. The error is statistical uncertainty. The values and errors are obtained from likelihood distribution.

DATA FIT IN BINS

A combined fit is performed to obtain the $B^0 \rightarrow DK^{*0}$ yield in each bin. The combined fit constrains the amount of the D true $B\bar{B}$ background in bins from the ratio of $D^0 (K_i)$ and $\bar{D}^0 (K_{-i})$ from the generic MC, the amount of the D fake $B\bar{B}$, $q\bar{q}$, $D^0 \rho^0$ and $D^0 a_1^+$ backgrounds in bins from the MC, and takes the (x_{\pm}, y_{\pm}) variables as free parameters. Fits to B^0 and \bar{B}^0 data are performed separately. The plots illustrating the combined fit results are given in the Appendix. In this fit, the additional free parameters are the total yields of D true $B\bar{B}$, D fake $B\bar{B}$, $q\bar{q}$ and peaking $B\bar{B}$ backgrounds for all over the Dalitz plane. The values of (x, y) parameters and their statistical correlations obtained from the combined fit for signal sample are given in Table II.

SYSTEMATIC UNCERTAINTY

The systematic uncertainties on (x, y) are obtained by taking variations from the default procedure under differing assumptions. Most systematic uncertainties are negligible compared to the statistical uncertainty. Therefore, numerical values are not given unless they are greater than or equal to 0.1 for any contribution. There is an uncertainty due to the Dalitz plot efficiency variation because of the difference in average efficiency over each bin for the flavor-tagged and $B^0 \rightarrow DK^{*0}$ samples. A maximum difference of 1.5 % is obtained in a MC study. The uncertainty is taken as the maximum of two quantities:

- the root mean square of x and y from smearing the numbers of events in the flavor-tagged sample K_i by 1.5%, or
- the bias on x and y between the fits with and without efficiency correction for K_i obtained from signal MC.

The uncertainty due to crossfeed of events between bins is estimated by taking the bias between the fits with and without the correction. The uncertainties due to the fixed parametrization of the signal and background PDFs are estimated by varying them by $\pm 1\sigma$. The uncertainty due to the C'_{NB} PDF distributions for $B\bar{B}$ are estimated by replacing them with the signal C'_{NB} PDF. The uncertainty due to D true and D fake $B\bar{B}$ fraction of yield is estimated by varying them from 0 to 1. The uncertainty due to PDFs shape is $(\Delta x_-, \Delta y_-, \Delta x_+, \Delta y_+) = (+0.0, +0.1, +0.0, +0.0)_{-0.1, -0.0, -0.1, -0.1}$. The uncertainty arising from the finite sample of flavor-tagged $D \rightarrow K_S^0 \pi \pi$ decays is evaluated by varying the value of K_i within their statistical uncertainties. The uncertainty due to the uncertainty on k in Eq. (2) is evaluated by varying the value of k within its error [16]. The uncertainty due to the limited precision of c_i and s_i parameters is obtained by smearing the c_i and s_i values within their total errors and repeating the fits for the same experimental data. The uncertainty due to c_i, s_i is $(\Delta x_-, \Delta y_-, \Delta x_+, \Delta y_+) = (\pm 0.0, \pm 0.1, \pm 0.1, \pm 0.1)$.

The total systematic uncertainty is $(\Delta x_-, \Delta y_-, \Delta x_+, \Delta y_+) = (+0.0, \pm 0.1, \pm 0.1, \pm 0.1)_{-0.1, -0.0, -0.1, -0.1}$. The systematic uncertainty without c_i, s_i is $(+0.0, +0.1, +0.0, +0.0)_{-0.1, -0.0, -0.1, -0.1}$.

RESULT FOR (x, y) AND r_S

We use the frequentist approach with the Feldman-Cousins ordering [26] to obtain the physical parameters $\mu = (\phi_3, r_S, \delta_S)$ (or true parameters $\mu = z_{\text{true}} = (x_-, y_-, x_+, y_+)$) from the measured parameters $z = z_{\text{meas}} = (x_-, y_-, x_+, y_+)$ taken from the likelihood distribution. In essence, the confidence level α for a set of physical parameters μ is calculated as

$$\alpha(\mu) = \frac{\int_{\mathcal{D}(\mu)} p(z | \mu) dz}{\int_{\infty} p(z | \mu) dz}, \quad (15)$$

where $p(z | \mu)$ is the probability density to obtain the measurement result z given the set of true parameters μ . The integration domain $\mathcal{D}(\mu)$ is given by the likelihood ratio (Feldman-Cousins) ordering:

$$\frac{p(z | \mu)}{p(z | \mu_{\text{best}}(z))} > \frac{p(z_0 | \mu)}{p(z_0 | \mu_{\text{best}}(z_0))}, \quad (16)$$

where $\mu_{\text{best}}(z)$ is μ that maximizes $p(z | \mu)$ for the given z , and z_0 is the result of the data fit. This PDF is taken from MC pseudo-experiments.

Systematic errors in μ are obtained by varying the measured parameters z within their systematic errors assuming a Gaussian distribution. In this calculation we assume that the systematic errors are uncorrelated between the B^0 and \bar{B}^0 samples.

As a result of this procedure, we obtain the confidence levels (C.L.) for (x, y) and the physical parameter r_S . The C.L. contours on (x, y) are shown in Fig. 3. The likelihood profile for r_S is shown in Fig. 4. The final results are:

$$x_- = +0.4_{-0.6-0.1}^{+1.0+0.0} \pm 0.0 \quad (17)$$

$$y_- = -0.6_{-1.0-0.0}^{+0.8+0.1} \pm 0.1 \quad (18)$$

$$x_+ = +0.1_{-0.4-0.1}^{+0.7+0.0} \pm 0.1 \quad (19)$$

$$y_+ = +0.3_{-0.8-0.1}^{+0.5+0.0} \pm 0.1, \quad (20)$$

$$r_S < 0.87 \quad \text{at 68\% C.L.} \quad (21)$$

CONCLUSION

We report the result of a measurement of the amplitude ratio r_S using a model-independent Dalitz plot analysis of $D \rightarrow K_S^0 \pi^+ \pi^-$ decay in the process $B^0 \rightarrow DK^{*0}$. The value of r_S indicates the sensitivity of the decay to ϕ_3 because the statistical uncertainty is proportional to $1/r_S$. The measurement was performed with the full data sample of 711 fb^{-1} (772×10^6 $B\bar{B}$ pairs) collected by the Belle detector at the $\Upsilon(4S)$ resonance. Model independence is achieved by binning the Dalitz plot of the $D \rightarrow K_S^0 \pi^+ \pi^-$ decay and using the strong-phase coefficients for bins measured by the CLEO experiment [18]. We obtain the value $r_S < 0.87$ at 68 % C.L.

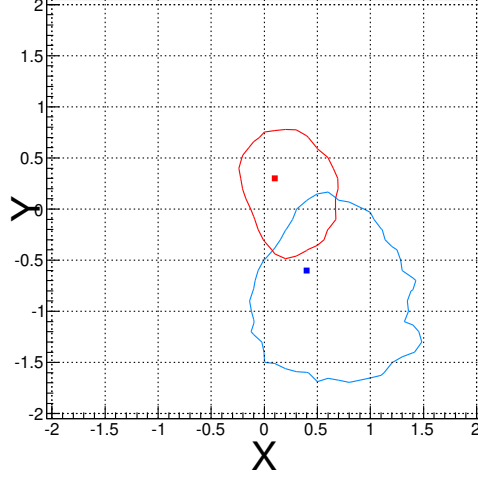


FIG. 3: C.L. on (x_-, y_-) (blue) and (x_+, y_+) (red). Dots show the most probable (x, y) values, lines show 68 % contours. The fluctuations come from statistics of pseudo-experiments and C.L. step used.

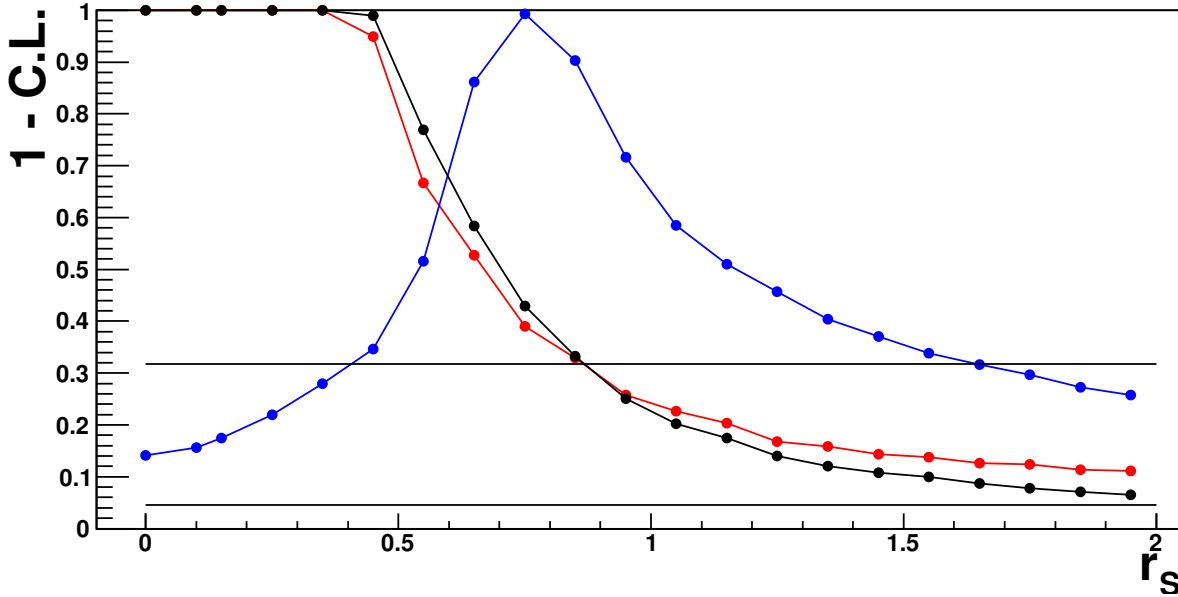


FIG. 4: Likelihood profile for r_S . Blue is for $\bar{B}^0 (x_-, y_-)$, red is for $B^0 (x_+, y_+)$ and black is \bar{B}^0 and B^0 combined.

This analysis is the first using the model-independent Dalitz technique on neutral B mesons. This measurement has resulted in lower statistical precision than the model-dependent measurement from BaBar with the $B^0 \rightarrow DK^{*0}$ mode [8] despite the larger data sample due to the smaller $B^0 \rightarrow DK^{*0}$ signal observed. The result is consistent with the most precise r_S measurement reported by the LHCb Collaboration [27] of $r_S = 0.240^{+0.055}_{-0.048}$ which uses $B^0 \rightarrow [K^+ K^-, K^\pm \pi^\mp, \pi^+ \pi^-]_D K^{*0}$ decays.

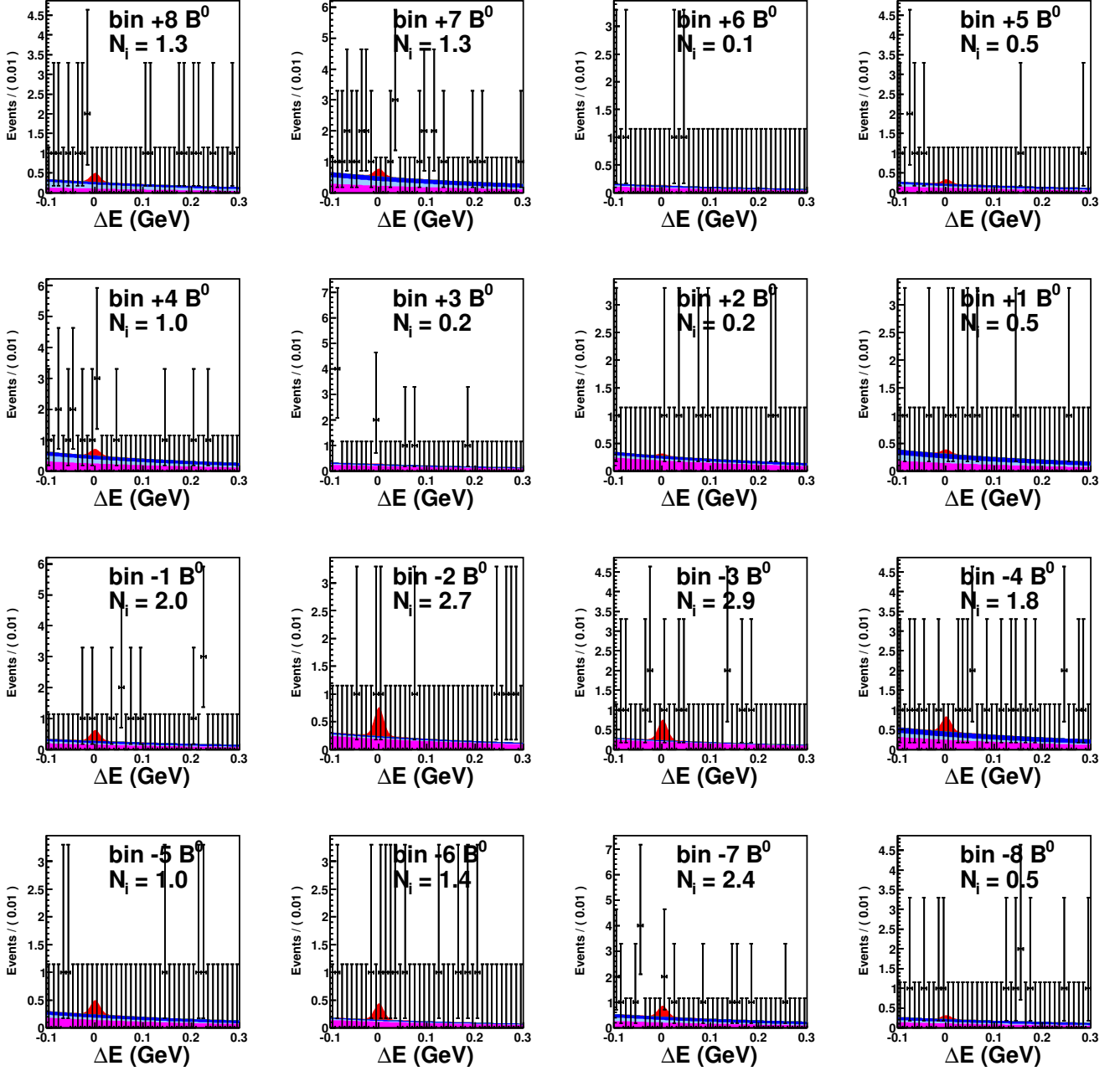


FIG. 5: Projections of the combined fit of the $B^0 \rightarrow DK^{*0}$ sample on ΔE for each Dalitz plot bin, with the $M_{bc} > 5270$ MeV/ c^2 and $C'_{NB} > 2$ requirements. The fill styles for the signal and background components are the same as in Fig. 2.

APPENDIX

The results of the combined fit to $B^0 \rightarrow DK^{*0}$ and $\bar{B}^0 \rightarrow DK^{*0}$ samples separately for each bin of the Dalitz plot are shown in Figs. 5 and 6, respectively. The plots show the projections of the data and the fitting model on the ΔE variable, with the additional requirements $M_{bc} > 5270$ MeV/ c^2 and $C'_{NB} > 2$.

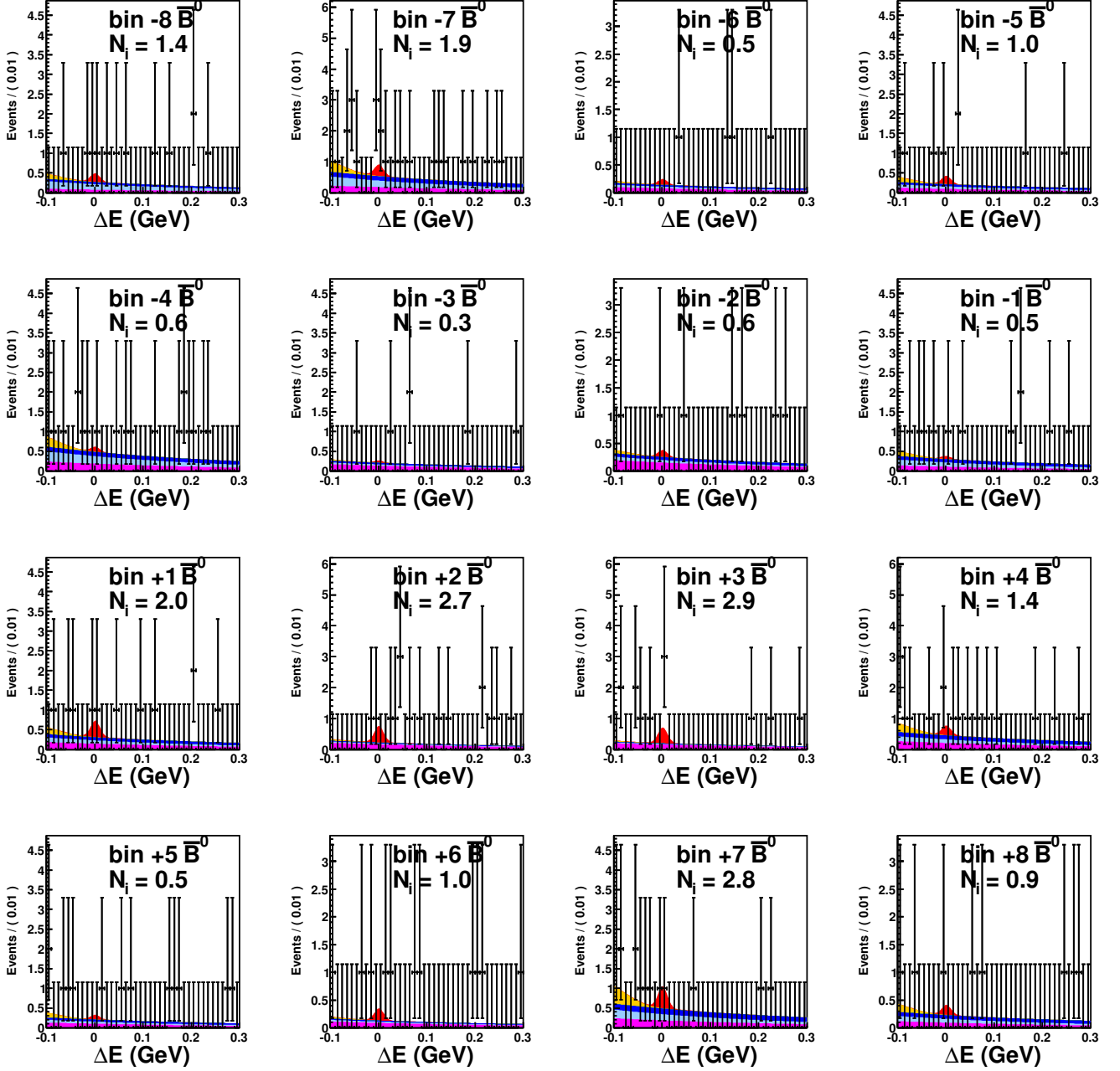


FIG. 6: Projections of the combined fit of the $\bar{B}^0 \rightarrow D\bar{K}^{*0}$ sample on ΔE for each Dailtz plot bin, with the $M_{bc} > 5270$ MeV/ c^2 and $C'_{NB} > 2$ requirements. The fill styles for the signal and background components are the same as in Fig. 2.

- [2] L. Wolfenstein, Phys. Rev. Lett. **51**, 1945 (1983).
- [3] K. Abe *et al.* (Belle Collab.), Phys. Rev. Lett. **90**, 131803 (2003).
- [4] T. Aaltonen *et al.* (CDF Collab.), Phys. Rev. D **81**, 031105 (2010).
- [5] A. Poluektov *et al.* (Belle Collab.), Phys. Rev. D **81**, 112002 (2010).
- [6] P. del Amo Sanchez *et al.* (BaBar Collab.), Phys. Rev. D **82**, 072004 (2010).
- [7] P. del Amo Sanchez *et al.* (BaBar Collab.), Phys. Rev. D **82**, 072006 (2010).
- [8] P. del Amo Sanchez *et al.* (BaBar Collab.), Phys. Rev. Lett. **105**, 121801 (2010).
- [9] T. Aaltonen *et al.* (CDF Collab.), Phys. Rev. D **84**, 091504 (2011).
- [10] Y. Horii *et al.* (Belle Collab.), Phys. Rev. Lett. **106**, 231803 (2011).
- [11] R. Aaij *et al.* (LHCb Collab.), arXiv:1203.3662 (2012).

- [12] B. Aubert *et al.* (BaBar Collab.), Phys. Rev. D **80**, 031102 (2009).
- [13] A. Giri, Y. Grossman, A. Soffer, and J. Zupan, Phys. Rev. D **68**, 054018 (2003).
- [14] H. Aihara *et al.*, (Belle Collab.), Phys. Rev. D **85**, 112014 (2012).
- [15] M. Gronau, Phys. Lett. B **557**, 198 (2003).
- [16] B. Aubert *et al.* (BaBar Collab.), Phys. Rev. D **79**, 072003 (2009).
- [17] R. A. Briere *et al.*, (CLEO Collab.), Phys. Rev. D **80**, 032002 (2009).
- [18] J. Libby *et al.*, (CLEO Collab.), Phys. Rev. D **82**, 112006 (2010).
- [19] A. Bondar and A. Poluektov, Eur. Phys. J. C **47**, 347 (2006).
- [20] A. Poluektov *et al.*, (Belle Collab.), Phys. Rev. D **81**, 112002 (2010).
- [21] S. Kurokawa and E. Kikutani, Nucl. Instr. and Meth. A **499**, 1 (2003), and other papers included in this volume.
- [22] A. Abashian *et al.* (Belle Collab.), Nucl. Instr. and Meth. A **479**, 117 (2002).
- [23] The Fox-Wolfram moments were introduced in G. C. Fox and S. Wolfram, Phys. Rev. Lett. **41**, 1581 (1978). The Fisher discriminant used by Belle, based on modified Fox-Wolfram moments (SFW), is described in K. Abe *et al.* (Belle Collab.), Phys. Rev. Lett. **87**, 101801 (2001) and K. Abe *et al.* (Belle Collab.), Phys. Lett. **B 511**, 151 (2001).
- [24] H. Kakuno *et al.*, Nucl. Instr. and Meth. A **533**, 516 (2004).
- [25] M. Feindt and U. Kerzel, Nucl. Instr. and Meth. A **559**, 190 (2006).
- [26] G. J. Feldman and R. D. Cousins, Phys. Rev. D **57**, 3873 (1998).
- [27] R. Aaij *et al.*, (LHCb Collab.), Phys. Rev. D **90**, 112002 (2014).